

MONTE CARLO METHODS IN ELECTRONIC STRUCTURES FOR LARGE SYSTEMS

Arne Lüchow

*Institut für Physikalische Chemie, Heinrich-Heine-Universität Düsseldorf, 40225
Düsseldorf, Germany; e-mail: luechow@uni-duesseldorf.de*

James B. Anderson

*Department of Chemistry, Pennsylvania State University, University Park, Pennsylvania
16802; e-mail: jba@psu.edu*

Key Words quantum mechanics, quantum Monte Carlo, quantum chemistry

■ **Abstract** Quantum Monte Carlo methods have recently made it possible to calculate the electronic structure of relatively large molecular systems with very high accuracy. These large systems range from positron complexes [NH₂,Ps] with ~10 electrons to C₂₀ isomers with 120 electrons, to silicon crystal structures of 250 atoms and 1000 valence electrons. The techniques for such calculations and a sampling of applications are reviewed.

INTRODUCTION

In the 10 years since the first review on quantum Monte Carlo (QMC) methods in this publication (1), these methods have made significant advances toward larger systems and higher accuracies. For systems of a few electrons, the accuracies achieved have inspired statements such as "... the results presented are impressive but seem unnecessarily precise for chemistry" (2). For systems with more than a few atoms, the accuracies achieved have inspired statements such as "... fixed-node DMC [diffusion Monte Carlo] is already much more accurate than any competing method" (3).

In this review we consider only the larger systems—those with more than a few atoms ... those which range from ~10 electrons (or particles) as for positron complexes [NH₂,Ps] ... to C₂₀ isomers with 120 electrons ... to silicon crystal structures of 250 atoms and 1000 valence electrons. We first introduce briefly the several available QMC methods, and then we focus on selected representative applications to large systems in different fields of physical chemistry and chemical physics.

Since the earliest days of quantum mechanics, the usual way of treating quantum effects in chemistry has been the reduction of all problems to one-body problems.

In the Hartree-Fock (HF) method, the complicated electron distribution of molecules is reduced to the movement of one electron in the mean field of the others. And for a normal-mode analysis, the interatomic forces are simplified such that one-dimensional vibrational equations result. Although these approximations lead to helpful visualizations of the orbitals and of the normal modes, quite often they lack quantitative agreement with experimental data. Many improvements based on one-body or one-dimensional theories, such as perturbation methods, have been developed. In classical theories, such as molecular dynamics or classical Monte Carlo, the many-body problem is directly attacked. In QMC methods, a “quantum simulation” is used to transfer this approach to quantum mechanical many-body problems. Quite generally, QMC methods may be applied advantageously to quantum systems with many coupled degrees of freedom. Consequently, QMC has been applied to electron correlation in molecules and solids and to vibrational motion in weakly bound systems.

QMC methods have been described in detail in a monograph (4) and a number of recent review articles that focus on electronic-structure (2, 5–9) and vibrational-structure (10) calculations. The use of random numbers in Monte Carlo calculations results in a statistical uncertainty, so that energies and other properties obtained with QMC methods have characteristic statistical error bars. In general, this statistical error decreases only slowly, as $1/\sqrt{N}$, with the number N of evaluations, but it does not generally depend on the dimensionality of the problem. This is the reason that the computational effort for QMC methods typically scales favorably with the system size. The various QMC methods differ in the application of the random numbers.

The scaling of computational effort with system size for QMC methods in general has been examined in several studies (3, 11, 12). For fixed-node diffusion QMC (FN-DQMC), the most often used method for large systems, the computation effort is primarily expended in evaluating determinants of size $N \times N$, where N is the number of electrons, and the scaling is very close to N^3 . This scaling behavior is observed for FN-DQMC calculations for clusters of 2–10 carbon atoms, as shown in Figure 1.

The scaling of effort with system size may be compared for several different types of electronic-structure calculations in Table 1. This table is adapted from a review in 1996 by Head-Gordon (13), and we have added the row for QMC. As noted by Head-Gordon, the scalings listed are very approximate. We note that linear scalings have been proposed for several methods. Thus, the table must be considered qualitative at best. Nevertheless, QMC is one of the very few methods that are useful for large systems.

DIFFUSION QUANTUM MONTE CARLO

The most widely used QMC method in chemistry is the diffusion QMC method DQMC (14). It is based on the mathematical equivalence of the time-dependent

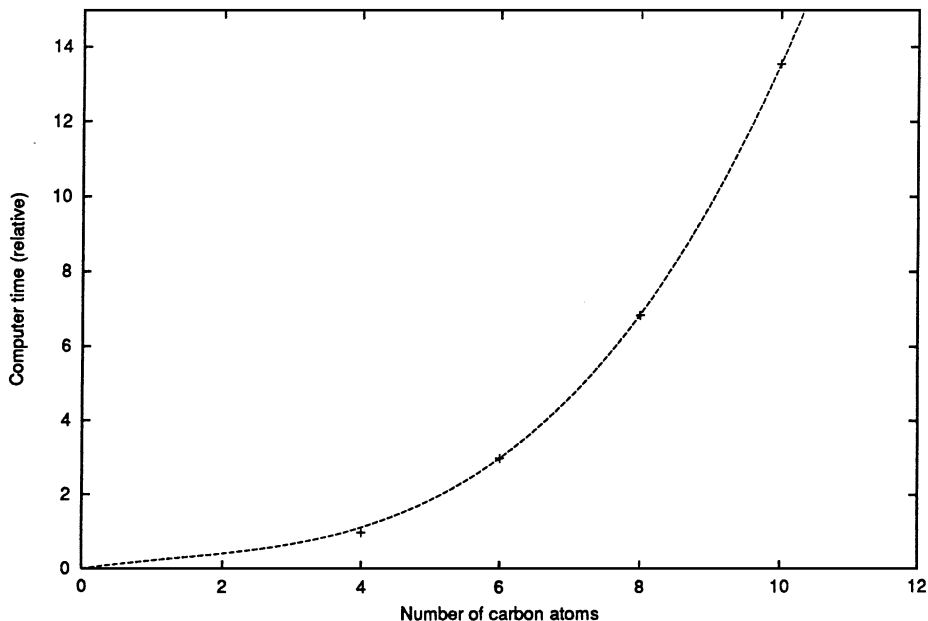


Figure 1 Scaling of quantum Monte Carlo computation effort with system size. The dotted line varies as N^3 . From reference 12 by permission.

Schrödinger equation in imaginary time $\tau = it$:

$$\frac{\partial \Psi(r, \tau)}{\partial \tau} = \frac{1}{2m} \nabla^2 \Psi(r, \tau) - V(r) \Psi(r, \tau), \quad 1.$$

with a generalized diffusion equation

$$\frac{\partial c(r, t)}{\partial t} = D \nabla^2 c(r, t) - k(r) c(r, t). \quad 2.$$

Here D is identified as the diffusion constant in Fick's second law and $k(r)$ as the position-dependent rate constant of a first-order rate equation. Fermi not only noticed, according to Metropolis & Ulam (15), the equivalence between Schrödinger's equation and the diffusion equation, but suggested also that a random walk in which a particle diffuses and simultaneously multiplies based on the rate constant would eventually give the ground-state wave function. Fermi's conclusion can be seen from the formal solution of the Schrödinger equation above, as follows:

$$\Psi(r, \tau) = e^{-\tau H} \Psi(r, 0), \quad \text{with } H = -\frac{1}{2m} \nabla^2 + V(r). \quad 3.$$

After expanding the initial wave function in eigenfunctions of H ,

$$\Psi(r, 0) = \sum_i a_i \Phi_i, \quad 4.$$

TABLE 1 Scaling of computation effort with molecular size^a

Theoretical method ^b	Current computational dependence on molecular size, M	Current estimate of maximum feasible molecular size
FCI	Factorial	2 Atoms
CCSD(T)	M^7	8–12 atoms
CCSD	M^6	10–15 atoms
MP2	M^5	25–50 atoms
HF, KS-DFT	M^2 – M^3	50–200 atoms
FN-QMC	M^3	250–500 atoms

^aAdapted from Head-Gordon (13) with additions from Shlyakhter et al (12).

^bFCI, CCSD(T), full configuration interaction coupled cluster method with perturbative triple excitation; CCSD, coupled cluster method; MP2, Møller-Plesset perturbation 2; HF, KS-DFT, Hartree-Fock, Kohn-Sham–density functional methods; FN-QMC, Fixed-node–quantum Monte Carlo.

the time-dependent solution is obtained in terms of eigenfunctions

$$\Psi(r, \tau) = \sum_i a_i e^{-E_i \tau} \Phi_i. \quad 5.$$

The contributions from higher states decay exponentially compared with the ground state. When a random walk satisfying the diffusion equation is constructed, the ground-state wave function is obtained exactly, after a sufficiently long time, as a distribution of random walkers. Quantum mechanical expectation values can be obtained as statistical expectation values.

In this form, the DQMC method can be applied to obtain zero-point energies and ground-state wave functions of vibrational Schrödinger equations. When this method is applied to electronic-structure problems, two difficulties are met; the Coulomb singularities in the electronic Hamiltonian prohibit an efficient simulation of the rate part, and the Pauli principle leads to nodes in the wave function for the ground state of systems with more than two electrons. The first problem is solved with an importance-sampling transformation (16) of the original Schrödinger equation, in which a guide function Ψ_G is introduced that guides the random walk toward regions where Ψ_G is large. The random walk then consists of a diffusion step as before, a new drift step with a velocity $\nabla \Psi_G / \Psi_G$, and a reaction term with the rate constant now $E_{loc} = H\Psi_G / \Psi_G$ (17). Umrigar et al could further improve the DQMC algorithm with a modified drift and multiplication step (18).

The second problem, the node structure of the physical ground-state wave function, is a manifestation of the general fermion sign problem. An approximation to the true ground state is obtained when the nodes of a nodal function are imposed on the random walk—the FN-DQMC (19). It can be shown that the resulting fixed-node energy is variational, that is, $E_{FN} \geq E_0$. Typically, the importance-sampling

guide function Ψ_G serves also to define the nodes. If Ψ_G satisfies the Pauli principle, then so too will the FN-DQMC solution Ψ_0 . A more accurate, but less efficient solution can be obtained in principle when the nodes are released from their fixed locations in released node QMC (20).

The error caused by the fixed-node approximation is smaller when the guide function is closer to the exact ground-state function. In many DQMC calculations, Ψ_G is of the form

$$\Psi_G = e^U \sum_k c_k \det(\Phi_k), \quad 6.$$

where $\det(\Phi_k)$ is a Slater determinant of HF or local density approximation (LDA) orbitals and U is a ‘‘Jastrow’’ term, depending explicitly on the electron-electron distances

$$U = U[(r_{ij})], \quad \text{with } r_{ij} = |r_i - r_j|, \quad 7.$$

to satisfy the electron cusp condition. Because the dynamic electron correlation is accounted for by e^U , one or only a few determinants in Ψ_G are used. The parameters of U are optimized by variance minimization with Monte Carlo methods (21). With guide functions of this type, >90% of the correlation energy is routinely obtained with FN-DQMC.

The efficiency of the DQMC method for atoms and molecules can be improved further through the use of pseudopotentials to replace the core electrons (PP-DQMC). Pseudopotentials work for DQMC in the same way as for other ab initio methods, but they have the additional benefit of reducing the statistical variance caused by the high-energy core electrons. Pseudopotentials in QMC have been introduced independently by Hurley & Christiansen (22) and by Hammond et al (23).

A further variant of DQMC is the rigid-body DQMC method (RB-DQMC), for vibrational motion in clusters, by Buch (24). To separate the high-frequency intramolecular modes from low-frequency intermolecular modes, a purely intermolecular Hamiltonian is used,

$$H_{RB} = T_{com} + T_{rot} + V_{inter}. \quad 8.$$

This equation contains the kinetic energy of the centers of mass of the monomers, the rotational energy of the monomers, and the intermolecular potential. The corresponding random walk without importance sampling consists of a diffusion step for the centers of mass, a random rotation about the axes of inertia, and a multiplication step that corresponds to the intermolecular potential. From the RB-DQMC calculation, the intermolecular zero-point energy and the vibrationally averaged geometry are obtained.

VARIATIONAL QUANTUM MONTE CARLO

An efficient QMC variant is the variational QMC method (VQMC). Here the Rayleigh-Ritz quotient,

$$E = \frac{\langle \Psi_T | H | \Psi_T \rangle}{\langle \Psi_T | \Psi_T \rangle} = \frac{\int \Psi_T^2 \frac{H\Psi_T}{\Psi_T} d\tau}{\int \Psi_T^2 d\tau}, \quad 9.$$

is evaluated with Monte Carlo integration. The energy E is variational: $E \geq E_0$. Usually, but not necessarily, Ψ_T^2 is sampled with the Metropolis algorithm (25). In this form, VQMC was first used by Conroy (21) for small molecules and by McMillan (26) for the ground state of liquid helium. In current VQMC applications, the generalized Metropolis algorithm (27) is used, thereby allowing directed steps such as the drift/diffusion step from the importance-sampled DQMC algorithm. This not only increases the efficiency of the VQMC method considerably, but it also makes DQMC and VQMC algorithms very similar, with VQMC being more efficient and less accurate. Because of its efficiency, VQMC is the method used for the largest QMC applications. In electronic-structure calculations, the trial function Ψ_T is often of the same form as the guide function Ψ_G in DQMC.

GREEN'S FUNCTION QUANTUM MONTE CARLO METHOD

The Green's function QMC method is based on the time-independent Schrödinger equation. This equation can be transformed into an integral equation (28, 29)

$$\Psi(r) = \int G(r, r') \frac{V(r)}{E} \Psi(r') dr'. \quad 10.$$

The Green's function $G(r, r')$ is known and can be sampled stochastically by using an ingenious algorithm from Kalos (29). In this way $G(r, r')$ is interpreted as a transition probability, and the integral equation can be realized with a random walk step. Iteration of the integral equation yields the ground state wave function. This algorithm has been used primarily for highly accurate calculations of few-electron systems.

REACTION PATHS FOR OXIDATION OF CYCLOPENTADIENE (36-VALENCE ELECTRONS)

Cyclopentadiene C_5H_6 is formed during the combustion process of aromatic compounds such as benzene (30, 31). Its further oxidation is a matter of great interest for the elucidation of combustion processes. In a recent study, Grossman et al (32) examined the oxidation of cyclopentadiene to 2-cyclopentenone and

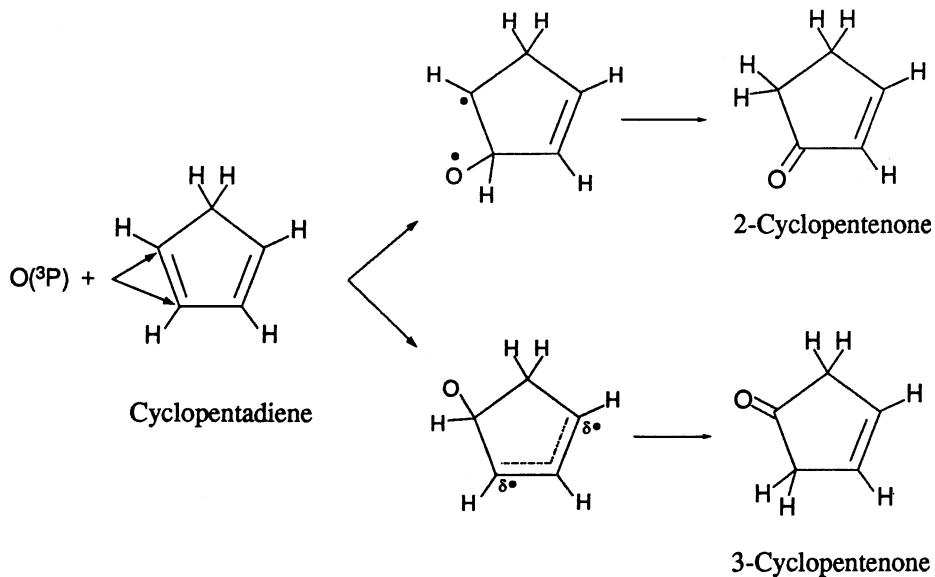


Figure 2 Reaction pathways for oxidation of cyclopentadiene to cyclopentenone. From reference 32 by permission.

3-cyclopentenone, which have been found in trace amounts during combustion. The authors used the PP-DQMC and the VQMC methods, as well as several density-functional methods and the coupled-cluster with perturbative triple excitation [CCSD(T)] method. In an earlier paper, the authors presented detailed PP-DQMC calculations on the cyclopentadiene reactant (33).

The reaction path considered in this study starts with the addition of a triplet oxygen to one cyclopentadiene double bond and reaches one of two possible diradical intermediates (Figures 2 and 3).

The reaction proceeds in each of the two channels via an intersystem crossing toward a singlet transition state and finally reaches the products 2- and 3-cyclopentenone. Grossman et al (32) used several ab initio methods to characterize the adduct, the diradicals, the transition states, and the products. The methods included PP-DQMC, CCSD(T), HF, and several density-functional (DFT) methods, based both on the local density approximation (LDA) and the generalized-gradient approximation, as well as the hybrid method B3LYP.

The geometries were optimized with a smaller basis set, but for the two high-level methods, CCSD(T) and PP-DQMC, an optimization was unfeasible, and the B3LYP DFT method was used instead. In calculations of the energies along the reaction path, results strongly varied with the method. Although the CCSD(T) method did not yield converged results, the PP-DQMC method was used to produce high-level energies for the diradicals and the transition states. Each of the methods

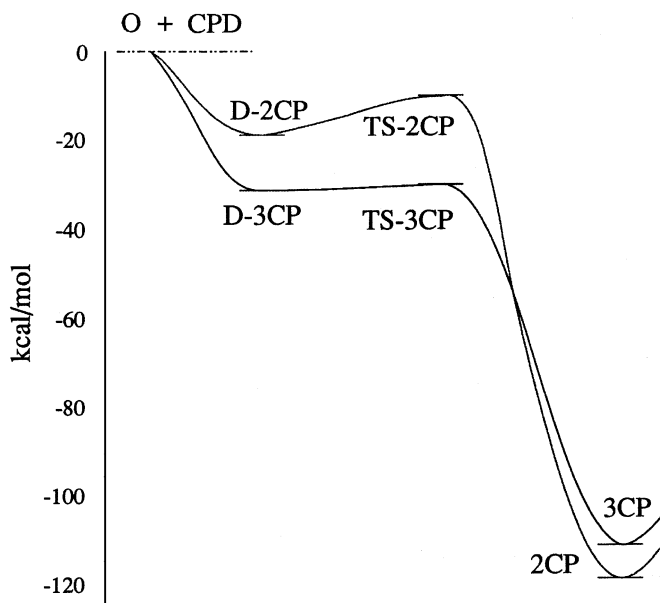


Figure 3 Energy diagram for oxidation of cyclopentadiene. CPD, cyclopentadiene; CP, cyclopentenone; D-, diradical intermediate; TS, transition state. From reference 32 by permission.

shows 2-cyclopentenone to be ~ 6 kcal/mol more stable than its isomer, although the energy of reaction varies strongly with the method.

In an assessment of the methods used in this study, it can be concluded that PP-DQMC provides highly accurate results, whereas CCSD(T) as a method of comparable accuracy could not be successfully applied for a system of this size. HF and DFT methods do not satisfactorily account for the electron correlation energy that contributes very importantly to the energetics of reactions for which the bonding pattern changes.

Assuming the PP-DQMC result as the most accurate in this study, the preferred formation of 3-cyclopentenone can be explained with the more stable diradical precursor and the smaller barrier.

INVERSION OF CYCLO-OCTATETRAENE (40 VALENCE ELECTRONS)

Cyclo-octatetraene (COT) with its eight π electrons is not aromatic and thus has a nonplanar D_{2d} structure. It has long been known that COT can undergo inversion between the degenerate D_{2d} structures. With new techniques it is now possible to measure barrier heights experimentally to high accuracy—thereby challenging

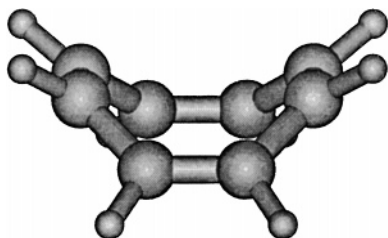


Figure 4 Cyclo-octatetraene in its D_{2d} ground state.

theoretical methods. The difference between the D_{2d} ground state of COT and its planar D_{8h} transition state has been measured to an accuracy of >2 kcal/mol (34). These configurations are shown in Figure 4 and Figure 5.

Grossman & Mitas (35) recently carried out PP-DQMC calculations for a number of different reaction systems to assess the accuracy of the method in predicting barrier heights for chemical reactions. Included among these was the D_{8h} barrier height for the COT inversion. An additional difficulty for the COT system is presented by the existence of an open shell singlet and a triplet transition state for the COT inversion. To account properly for the open shell singlet state, a generalized valence bond (GVB) trial wave function, a simple multideterminant function, was used for QMC. The QMC result is compared with the GVB method and several DFT methods. The system was too large for calculations with the high-level CCSD(T) method, using sufficiently large basis sets. The results in Table 2 show perfect agreement of the QMC calculation with the experimental data, whereas GVB and DFT methods give the wrong order of singlet and triplet.

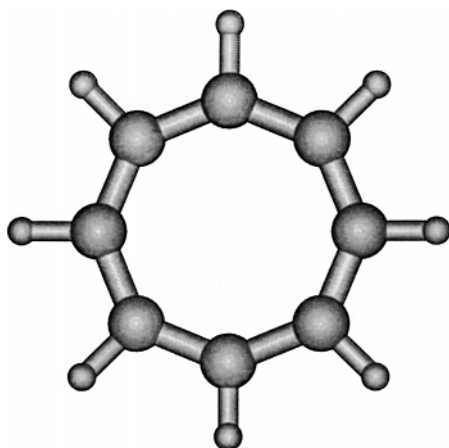


Figure 5 D_{8h} transition state for cyclo-octatetraene inversion.

TABLE 2 Energy differences in eV from D_{2d} ground state of cyclooctatetraene to singlet and triplet transition states^a

Method	TS singlet ^b	TS triplet ^b
GVB	1.40	1.19
LDA	0.95	0.67
BLYP	0.85	0.52
BPW91	0.88	0.50
QMC	0.61 (7)	0.87 (7)
Expt	0.61 (7)	0.95 (7)

^aReprinted from reference 35 by permission of the publisher. Numbers in parentheses indicate statistical error in last digit.

^bTS, Transition state; GVB, generalized valence bond; LDA, local density approximation; BLYP, hybrid method (Becke, Lee, Yang, Perdew); BPW91, Becke, Perdew, Wang, 1991; QMC, quantum Monte Carlo; Expt, experimental measurement.

C_{20} ISOMERS (120 ELECTRONS)

Carbon clusters of various sizes—and particularly the C_{20} clusters—provide an interesting and challenging testing ground for the variety of theoretical methods available to the physical chemist. In the range of C_4 to C_{32} , there exist several low-energy structures of each size, probably metastable, that differ in energies by only a few electron volts. The prediction of the lowest-energy, most stable structure requires accuracies in energy that are difficult to achieve for clusters larger than about C_{10} . Several reviews of experimental and theoretical work on carbon clusters are available (36–38).

The clusters C_8 and C_{10} are small enough for most of the electronic-structure methods listed in Table 3 (39–48). High-level Møller-Plesset perturbation (MP2 and MP4), configuration interaction singles, doubles, and triples [CISD(T)], and coupled-cluster CCSD(T) calculations, as well as PP-DQMC and all-electron FN-DQMC calculations, agree very well with each other in predicting the relative energies of the isomers of C_8 and C_{10} (12).

At the size of C_{20} , the effects of scaling of computational effort with system size limit the accuracies one may achieve with any of the methods. Some of the potentially accurate methods are limited to relatively small basis sets. Throughout the 1990s, the several methods gave conflicting results in predicting the relative energies for isomers of C_{20} .

The most stable isomers of C_{20} are the ring, bowl, and cage structures shown in Figure 6. Results from a variety of calculations for the relative energies of these three structures are listed in Table 3. In general, HF calculations favor the ring, MP2 favors the cage, simple DFT theory favors the cage, higher-level DFT

TABLE 3 Relative energies of isomers of C₂₀ in eV

Method ^a	Reference(s)	Type ^b	Ring ^c	Bowl ^c	Cage ^c
Semiempirical	46	AM1	<u>0.0</u>	14.7	12.5
HF and SCF	40	SCF	0.0	—	4.6
	41	HF	<u>0.0</u>	1.4	4.4
	43	SCF	<u>0.0</u>	0.2	2.2
	44, 44a	SCF	<u>0.0</u>	0.2	2.2
	45	HF	<u>0.0</u>	1.4	4.0
	47	HF	<u>0.0</u>	1.1	3.6
	47	HF	<u>0.0</u>	0.5	2.7
MP2	40	MP2	3.2	—	0.0
	43	MP2	2.8	1.1	<u>0.0</u>
	44, 44a	MP2	2.8	1.1	<u>0.0</u>
Density functional	39	LDA	2.2	0.8	<u>0.0</u>
	42	LDA	4.3	1.1	<u>0.0</u>
	44, 44a	LDA	2.3	0.8	<u>0.0</u>
	45	LDA	3.8	1.0	<u>0.0</u>
	47	LDA	3.9	1.5	<u>0.0</u>
	39	GC-LDA	<u>0.0</u>	0.7	1.7
	45	BLYP/HF	<u>0.0</u>	0.6	3.8
	45	BLYP	<u>0.0</u>	1.1	3.4
	47	BLYP	<u>0.0</u>	1.5	3.3
	42	BLYP	<u>0.0</u>	1.1	3.4
	42	BLYP	<u>0.0</u>	0.4	2.3
	43	BLYP	<u>0.0</u>	0.5	1.4
	42	BPW91	0.5	<u>0.0</u>	0.8
	42	BPW91	0.8	<u>0.0</u>	0.7
Coupled Cluster	43	CCSD	1.5	<u>0.0</u>	0.7
	43	CCSD(T)	1.7	<u>0.0</u>	<u>0.0</u>
	44, 44a	CCSD(T)	1.7	<u>0.0</u>	<u>0.0</u>
	44, 44a	CCSD(T)+	3.0	0.7	<u>0.0</u>
Other	41	LMP2	1.8	<u>0.0</u>	1.4
	41	GVB-LMP2	1.0	<u>0.0</u>	2.7
	41	PS-J1	1.2	<u>0.0</u>	2.2
Quantum Monte Carlo	42	ppQMC	1.1	<u>0.0</u>	2.2
	48	aeQMC	1.0	<u>0.0</u>	2.0

^aAbbreviations : HF, Hartree-Fock; SCF, self-consistent field; MP2, Møller-Plesset second-order perturbation.

^bAbbreviations: AM1, Austin Model 1; LSD, LDA, local density approximation; GC, gradient corrected; BLYP, Becke, Lee, Yang, Perdew hybrid method; BPW91, Becke, Perdew, Wang 1991; CCSD, couple cluster method; CCSD(T), couple cluster method with perturbative triple excitation; LMP2, local Møller-Plesset; GVB, generalized valence bond; PS-J1, pseudospectral MP2 with adjusted parameters; PPQMC, pseudopotential quantum Monte Carlo; aeQMC, all-electron quantum Monte Carlo.

^cLowest values are underlined.

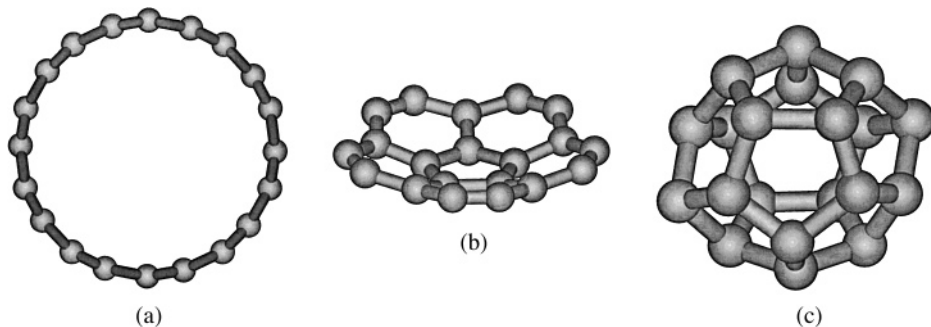


Figure 6 C_{20} isomers: *a*, ring; *b*, bowl; and *c*, cage. From reference 48 by permission.

favors both ring and bowl, CCSD and CCSD(T) favor the bowl and cage, local Møller-Plesset favors the bowl, and pseudospectral MP2 theory favors the bowl. Both PP-DQMC and all-electron FN-DQMC favor the bowl—agreeing quantitatively with each other and with the pseudospectral method.

We are perhaps not unbiased, but we believe the results of the two QMC calculations to be the most reliable. The QMC methods used for C_{20} are essentially the same as those found to be successful for C_8 and C_{10} .

Additional PP-DQMC calculations have been reported recently for carbon clusters C_{24} , C_{26} , C_{28} , and C_{32} (49).

DOPED HELIUM CLUSTERS (TO 500 PARTICLES)

Small superfluid ^4He droplets have attracted increasing interest recently. Molecules can be picked up (adsorbed or absorbed) easily by helium droplets in molecular beams to form doped helium clusters. With laser spectroscopic techniques, the dopant molecules can then be studied with high resolution at extremely low temperatures. Experiments show free rotor spectra for the molecules picked up by $^4\text{He}_N$ droplets, in contrast to nonsuperfluid fermionic $^3\text{He}_N$ clusters for which rotationally resolved spectra could not be obtained (50–53). With this technique it has become possible to form and study spectroscopically van-der-Waals clusters inside helium droplets (53, 54).

In a thorough theoretical description of doped helium clusters, the quantum nature of the clusters and the intrinsic many-body interactions inside the cluster pose a serious challenge. The QMC method is particularly well suited for this task, and it allows one to obtain the ground-state wave function exactly, provided that the interactions inside the cluster are known. Besides the determination of the structure of doped helium clusters, QMC-based methods can be used to investigate the influence of the cluster environment on the spectral properties of the dopant.

${}^4\text{He}_N\text{SF}_6$ was the first cluster explored with high-resolution spectroscopy (50), and it has sparked several theoretical studies of the question of the location of SF_6 inside the cluster and of the spectral shift of its vibrational modes. In both VQMC and DQMC calculations, Barnett & Whaley (55) found SF_6 to be near the center of the He cluster although increasingly delocalized with increasing cluster size, a fact confirmed by later studies with cluster sizes up to $N = 499$ (56). The central location of the dopant is in agreement with the fact that the SF_6 -He interaction is about sixfold as strong as the He-He interaction. It was also found that the first, fairly strongly bound solvation shell comprises ~ 22 He atoms. In VQMC and DQMC calculations, the zero-temperature structure is obtained, but path integral calculations can yield the temperature-dependent structure of clusters. Such calculations have been carried out by Kwon et al (57) for the cluster ${}^4\text{He}_{39}\text{SF}_6$. In these, the central dopant location was confirmed for $T = 0.625$ K and $T = 1.25$ K, and it was found that, despite the small cluster size and the strong SF_6 -He interaction, the cluster showed superfluid behavior at the lower temperature.

Lee et al (58) reported calculations of the rotational spectra of ${}^4\text{He}_N\text{SF}_6$ clusters with $1 \leq N \leq 20$, using a new DQMC variant called fixed-frame diffusion Monte Carlo, in which the rotationally excited states are obtained in the fixed-node approximation. The excitation energies are calculated with correlated sampling. In this work the decrease of the rotational constant B with the cluster size was calculated, and it could be shown that the experimental value $B = 0.033 \text{ cm}^{-1}$ for droplets with $N \geq 1000$ is already obtained with a cluster size of $N = 8$ and is constant for larger N . The conclusion, backed by analysis of the wave function, is that only a fraction of the first solvation shell can follow the SF_6 rotation and that this fraction consists of those atoms close to the minima of the potential energy surface, which are eight sites along the threefold axes of the SF_6 octahedron.

Other doped helium clusters have been calculated with QMC methods as well. Using VQMC, Barnett & Whaley (59) investigated ${}^4\text{He}_N\text{H}_2$ and found the hydrogen molecule being delocalized in clusters larger than $N \approx 20$ and behaving like an He atom. This can be rationalized by the fact that the He- H_2 interaction energy is comparable with the He-He interaction energy.

A dopant studied by several groups is the chlorine molecule Cl_2 . Its interaction strength with the helium atom is half that of SF_6 , and thus a stronger delocalization is expected. Bacic et al (60) used the Green's function QMC approach to calculate the small clusters He_2Cl_2 and He_3Cl_2 , finding both to be very floppy with large zero-point energies. McMahon & Whaley (61) investigated He_NCl_2 with $N = 1, 6,$ and 20 and found a ring of He atoms around the chlorine bond axis at $N = 6$ and a closed first solvation shell for $N = 20$. All clusters have large zero-point energies and are quite floppy, although in each case the chlorine is located, if delocalized, in the center.

Blume et al (62) calculated the red shift of the HF vibrational frequency caused by the He environment in He_NHF clusters with up to $N = 198$ He atoms. These

authors used both VQMC and DQMC and found a red shift of $2.7 \pm 0.1 \text{ cm}^{-1}$ for clusters with $N > 100$. This is in excellent agreement with the measured shift of $2.65 \pm 0.15 \text{ cm}^{-1}$ (62) for clusters with >1000 atoms.

To summarize, the QMC methods allow an accurate investigation of structure and spectral properties of doped He_N clusters with $N \leq 500$.

POSITRON COMPLEXES [OH,Ps], [CH,Ps], AND [NH₂,Ps] (8–10 ELECTRONS AND 1 POSITRON)

The leptonic structures and stabilities of the ground state and several excited states of positronium hydride PsH (where Ps = e^+ , e^-) have been successfully treated in several VQMC and DQMC studies (63). The ground states of several positron-molecule and positronium-atom complexes involving first-row atoms have been similarly treated in VQMC and FN-DQMC studies (64, 64a). An example of these kinds of calculations is the work recently reported by Bressanini et al (65) for the systems [OH,Ps], [CH,Ps], and [NH₂,Ps], which each contain 8–10 electrons and 1 positron, as well as heavier nuclei. Earlier calculations for these and/or related species have been carried out using HF (66), MP2 (67, 68), and QMC (68, 69) methods.

The systems are equivalent to the molecules H₂O, CH₂, and NH₃ with one H atom in each replaced by Ps. The low mass of the positron requires that it be treated in the same manner as an electron rather than clamped like a proton in a typical electronic-structure calculation.

Bressanini et al (65) compared VQMC and FN-DQMC calculations for the set OH, OH⁻, and [OH,Ps]; the set CH, CH⁻, and [CH,Ps]; and the set NH₂, NH⁻, and [NH₂,Ps] (70, 71; Table 4). The calculations were carried out with explicitly correlated guide functions consisting of Slater determinants for the electrons, along with Schmidt-Moskowitz (72) correlation functions and, as required, an additional electron-positron correlation term. The guide function is given by

$$\Psi_G = \det(\phi_\alpha) \det(\phi_\beta) e^{U(r_{ee})} \Omega(r_p, r_{ep}), \quad 11.$$

where e^U is the electron-electron correlation term and Ω is the electron-positron correlation term. Optimizations of the correlation functions were accomplished by minimizing the variances of the local energies for fixed sets of configurations.

The nuclear geometries for the neutral molecules and their anions were obtained from either experimental information or from independent ab initio calculations. The nuclear geometries for the positron complexes were specified as those of the anions. Results are listed in Table 4.

The results permit the calculation of the vertical positron affinity for each neutral species and the binding energy for each of the complexes, as well as the electron affinity for each of the neutral species. The latter permits an assessment of the accuracy of the calculations through comparisons with experimental values of the electron affinities. These are all listed in Table 4.

TABLE 4 Variational and Fixed-node diffusion quantum Monte Carlo positron affinity (PA) and positronium binding energy (BE) for the complexes [M,Ps]

Molecule and state	E_{DQMC}	PA_{DQMC}	BE_{DQMC}	EA_{DQMC}	EA_{exp}^a
OH $^2\Pi$	-75.7213(8) ^c				
OH ⁻ $^2\Pi$	-75.722(2)				
[OH,Ps] $^{2,1}\Sigma^+$	-75.9815(9)	0.1941(10)	0.0102(12)	0.0661(9)	0.0673
CH $^2\Pi$	-38.4630(5) ^c				
CH ⁻ $^3\Sigma$	-38.5087(1)				
[CH,Ps] $^{2,3}\Sigma^-$	-38.7291(3)	0.2200(4)	0.0161(6)	0.0461(5)	0.0456
NH ₂ 2B_1	-55.7428(9)				
NH ₂ ⁻ 1A_1	-55.7218(11)				
[NH ₂ ,Ps] $^{2,1}A_1$	-55.9282(5)	0.2277(7)	0.0056(9)	0.0279(9)	0.0272

^aFN-DQMC and experimental electron affinity (EA) for the molecules OH, CH, and NH₂. Energies in Hartrees. From Bressanini et al (65). Numbers in parentheses indicate statistical error in last digit.

^bReference 70.

^cReference 71.

The calculated electron affinities give quite good agreement with the experimental values. The other results show ground-state [OH,Ps] and [CH,Ps] to be stable complexes. Ground-state [NH₂,Ps] is also found to be stable (but less so, and possibly unstable after consideration of zero-point energy). Compared with earlier calculations of several types, these QMC calculations have greater recoveries of correlation among electrons and between electrons and the positron. For this reason, one may expect the QMC-based predictions of the stabilities of the complexes to be the most reliable.

METALLO-CARBOHEDRENES (16 OUTER ELECTRONS FOR TiC)

The discovery of the titanium carbon cluster Ti₈C₁₂ by Guo et al (73) has initiated a large number of experimental (74, 75) and theoretical (76–78) investigations of this and similar compounds that have become known as metallo-carbohedrenes (Met-Cars). The proposed structures for this and related clusters, a cagelike pentagonal dodecahedron and a tetracapped tetrahedral cage structure, can explain their unusual stability (73, 78).

While electronic-structure calculations on Met-Cars are possible with DFT methods, the number of electrons is currently too large for high-level ab initio methods such as CCSD(T), multireference configuration interaction (MRCI), or FN-DQMC. The diatomic TiC is the simplest compound for studying bonding in Met-Cars and comparing methods as an initial step toward reliable theoretical investigation of Ti₈C₁₂ and similar clusters.

The diatomic TiC has been investigated with CCSD(T) and MRCI by Hack et al (79) and with PP-DQMC by S. Sokolova and A. Lüchow (80). Because electronic-structure calculations of transition metal compounds are much less standard than such calculations for first- and second-row elements, an assessment of the accuracy of the different ab initio methods is necessary. Owing to the lack of experimental data for TiC itself, the comparison of calculated and experimental excitation energy for the Ti atom is very valuable. The experimental ground state is $3d^24s^2\ ^3F$ and the $3d^34s^1\ ^5F$ state is known to be only 0.69 eV above the ground state (81). Although several DFT methods predict the quintet state as the ground state and a calculated HF energy difference is fortuitously in agreement (0.8 eV) with the experiment (79), the high-level MRCI and CCSD(T) methods overestimate the energy gap by >50% (79) despite large and carefully chosen basis sets. In the PP-DQMC calculations (80) for Ti and TiC, a neon core was used for Ti, and thus 12 of the Ti electrons were treated explicitly. Except for node-location error, there is no basis set error for DQMC, and >90% of the electron correlation energy has been obtained consistently with this method. The good agreement of the PP-DQMC excitation energy of 0.77 (2) eV with the experimental value is thus probably not due to fortuitous cancellation of errors. Both the $^1\Sigma$ and the $^3\Sigma$ states of TiC have been calculated with the same methods as for the Ti atom. The singlet state has low lying excited states and cannot properly be described with one determinant. The use of several determinants poses no problem to the PP-DQMC method. With multideterminant PP-DQMC, the $^3\Sigma$ state is 0.5 eV more stable than the $^1\Sigma$ state, whereas MRCI calculates a gap of only 0.16 eV. The dissociation energy D_e for both states is 0.5 and 0.3 eV, respectively, larger with PP-DQMC than with MRCI, which may hint to an insufficiently saturated basis set for the MRCI calculations.

WATER CLUSTERS [TO (H₂O)₁₀]

Water clusters have been the focus of considerable interest in recent years. One of the objectives is to understand how the properties of (H₂O)_n evolve toward the condensed phase. Small water clusters offer unique opportunities to study in detail, experimentally and theoretically, the structure and dynamics of the hydrogen-bonded network that determine the properties of liquid water.

On the experimental side, new techniques have made it possible to obtain rotational constants for small water clusters, with vibration-rotation-tunneling spectroscopy (82, 83) and infrared spectra in the OH stretch region (84–86). On the theoretical side, much progress has been achieved in the quest for an accurate water-water potential. In addition, the development of the rigid-body (RB) variant of the DQMC method by Buch (87) has allowed evaluation of the effect of the intermolecular zero-point motion on structure and energetics of small water clusters.

Gregory & Clary (88) applied the RB-DQMC method to the water hexamer and calculated exactly the zero-point energy for the given potential. They found the

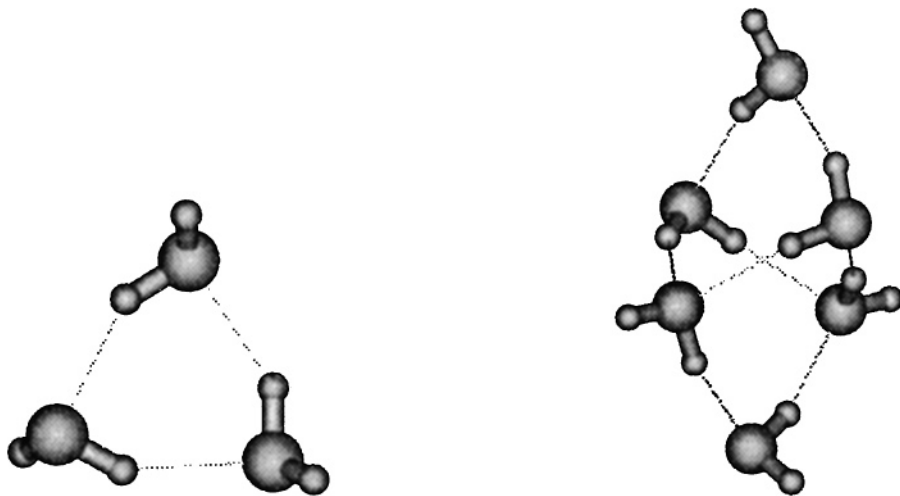


Figure 7 Water trimer cyclic (*left*) and water hexamer cage (*right*) structures. From reference 88 by permission.

cage structure (Figure 7) of the hexamer to be more stable than a prism structure when zero-point energies were included. Neglect of the zero-point energies leads to a prism structure as the most stable structure. The cage structure calculated by Gregory & Clary is in agreement with the rotational constants from the experiments by Liu et al (83). The water hexamer is thus the smallest noncyclic water cluster.

Larger water clusters $(\text{H}_2\text{O})_n$ up to the decamer ($n = 10$) have been investigated with the RB-DQMC method by Buch and coworkers (85, 86, 89). As for the water hexamer, the zero-point energy differences contribute considerably to the relative stabilities. The heptamer was found to be rather flexible and “liquid-like,” whereas the octamer was found to be more crystalline in behavior.

For each water cluster structure, many identical structures can be obtained by exchanging hydrogen atoms. Some of these exchange paths are physically feasible and lead to tunneling splittings in the IR spectra. In particular, the torsional motion of free OH can lead to identical structures with low barriers (90). QMC can be efficiently used for calculating tunneling splittings when the node on top of the tunneling barrier is enforced via the fixed-node method. QMC was first applied to the tunneling splitting of $(\text{HF})_2$ (91, 92). For the cyclic water trimer (Figure 7), Gregory & Clary used the RB-DQMC variant to calculate the tunneling splitting for different tunneling pathways (88).

More generally, DQMC can be used for the calculation of low-lying excited states in the fixed-node approximation provided that good approximate node locations are available. With DQMC, all intermolecular degrees of freedom are treated as fully coupled, thereby allowing the investigation of expected and unexpected couplings of normal modes. Severson & Buch (93) applied FN-DQMC to the

intermolecular vibrational states of the water hexamer, using nodal functions based on normal coordinates. They optimized the node locations and found strong reduction of several vibrational frequencies compared with the corresponding harmonic frequencies.

Finally, QMC has been used to study the effect of the zero-point motion on the dipole moment of the water molecule within water clusters (94). Because the average dipole moment of the water molecule in liquid water is $\sim 40\%$ larger than its value in the gas phase, the detailed investigation of its dipole moment within clusters is of considerable interest. The RB-DQMC method allows the determination of the effect of vibrational averaging on the magnitude and the direction of the dipole moment vector (95).

BAND STRUCTURE OF SILICON (64 VALENCE ELECTRONS)

In recent years, the QMC method has increasingly been applied to solids. QMC has many features that make it attractive for solid-state calculations: it scales reasonably with the number of explicitly treated electrons, and it can reliably calculate $>90\%$ of the electron correlation energy. It can be expected that QMC yields accurate cohesive energies. In QMC, as in other methods, the infinite nature of the solid is accounted for by periodic boundary conditions.

In the first QMC calculations for solids, Fahy et al (96, 97) were able to calculate the cohesive energy of diamond, graphite, and silicon with the variational QMC method. To determine the band structure of a solid, excitation energies have to be calculated. Mitas & Martin (98) used DQMC for calculating an energy gap in solid molecular nitrogen, and Mitas (99) calculated the $\Gamma_{25'} \rightarrow X_{1c}$ and $\Gamma_{1v} \rightarrow X_{1c}$ excitations in diamond. The states in these examples are special because they are the lowest states of their respective symmetry. For these, a guide function Ψ_G of appropriate symmetry is sufficient for the calculation of the lowest state of this symmetry within the FN-DQMC approximation. Although in most QMC applications, the ground-state wave function is calculated, excited states can also be calculated provided that an appropriate trial wave function is available (for VQMC) or approximately correct node locations for the excited state can be constructed (for DQMC). Williamson et al (100) calculated the band structure of silicon with the FN-DQMC method at the Γ , X , and L wave vectors. They constructed the guide wave functions for the excited states by replacing an orbital in the Slater determinant with a conduction band orbital. The orbitals are obtained from LDA calculations.

The guide function in this work (100) is more general than that of previous QMC calculations for solids (101). This approach has been termed “special k point method” and leads to smaller fixed-node errors. The results for the band energies of silicon are shown in Table 5, in comparison with calculations that use the LDA, HF (102), and GW (103) methods and to experimental data (104).

TABLE 5 Band energies of silicon in eV^a

Band	DQMC	HF	GW	LDA	Expt
$\Gamma_{25'}$	0.00	0.0	0.00	0.00	0.00
Γ_{15}	3.70	8.0	3.36	2.55	3.40, 3.05
$\Gamma_{2'}$	4.57	9.0	3.89	3.19	4.23, 4.1
Γ_1	-13.58	-18.9	-11.95	-11.95	-12.5 \pm 0.6
X_{1c}	1.51	5.3	1.43	0.63	1.25
X_4	-3.35	-4.7	-2.93	-2.84	-3.3 \pm 0.2, -2.9
X_{1v}	-8.79	-12.5	-7.95	-7.81	n/a
L_{1c}	2.51	6.5	2.19	1.44	2.4 \pm 0.15, 2.1
L_3	4.55	8.7	4.25	3.31	4.15 \pm 0.2
$L_{3'}$	-1.32	-2.0	-1.25	-1.19	-1.2 \pm 0.2, -1.5
L_{1v}	-7.81	-11.1	-7.14	-6.99	-6.7 \pm 0.2
$L_{2'}$	-11.05	-15.4	-9.70	-9.61	-9.3 \pm 0.4

^aThe DQMC entries have a statistical error of 0.2 eV. Republished from 100, by permission. Abbreviations: DQMC, diffusion quantum Monte Carlo; HF, Hartree-Fock; GW, Green's function/screened Coulomb; LDA, local density approximation; Expt, experimental data; n/a, not applicable.

Recently, a different approach for obtaining excitation energies with QMC has been developed (105), in which the extended Koopmans' theorem (106, 107) is used. This approach requires the density matrix $\rho(r; r')$ to be expanded in terms of LDA orbitals. The matrix elements ρ_{ij} of the density matrix are calculated as Monte Carlo expectation values during a VQMC run (105). With this VQMC-based method, many band energies for silicon have been calculated (105), in very good agreement with the previous DQMC results (100) and experimental data.

CUBIC BORON NITRIDE CRYSTALS (216 VALENCE ELECTRONS)

Malatesta et al (108) have carried out VQMC calculations to investigate the cohesive properties of cubic boron nitride crystals. These PP-VQMC calculations were made for simulation regions of $2 \times 2 \times 2$ and $3 \times 3 \times 3$ unit cells of two atoms (B-N) with totals of 64 and 216 valence electrons, respectively. The properties calculated were found in good agreement with experiments.

Cubic boron nitride is a prototypical heteropolar system, similar in many ways to diamond. The calculation procedures that were successful in earlier calculations for diamond were similarly successful for boron nitride. The pseudopotentials were of the Hamann-Schlüter-Chiang type (109) used in earlier calculations

TABLE 6 Results of variational quantum Monte Carlo calculations for the cubic BN crystal^a

Ground-state energy	VMC (eV)	LDA (eV)	Expt ^b (eV)
B atom	-71.31 ± 0.014	-70.55	
N atom	-266.57 ± 0.014	-264.95	
cBN ($2 \times 2 \times 2$)	-349.11 ± 0.09	-348.60	
cBN ($3 \times 3 \times 3$)	-350.70 ± 0.08	-350.54	
cBN (size-corrected)	-351.06 ± 0.08	-350.90	
Cohesive energy	12.85 ± 0.09	15.07	12.9–13.0

^aCalculations are by Malatesta et al (108). Energies are in eV for B and N and in eV per pair of atoms for the crystal. Calculated cohesive energy includes added zero-point energy of 0.33 eV per pair.

^bExperimental data are from reference 110.

for diamond. The boron nitride crystals lack the inversion symmetry of diamond and required somewhat different Jastrow terms for the Slater-Jastrow importance-sampling functions.

Results are listed in Table 6 and include ground-state energies for the free atoms B and N, as well as those for $2 \times 2 \times 2$ and $3 \times 3 \times 3$ primitive unit cells of the equilibrium crystal lattice for the VQMC and companion LDA density functional calculations. Finite-size corrected values, with the corrections derived from the LDA calculations, are also listed. The cohesive energies determined for the BN pairs are listed and may be compared with that derived from experiments (110). The lattice constant that is determined from the VQMC calculations is $3.58 \pm 0.04 \text{ \AA}$, which is in good agreement with the experimental value (110) of $3.615 \pm 0.002 \text{ \AA}$.

The VQMC calculations of cohesive and structural properties for this system of two different atoms were found to give excellent results.

DIAMOND STRUCTURE SILICON (TO 1000 VALENCE ELECTRONS)

The largest system treated to date in QMC calculations is a 250-atom extended system of silicon atoms in a diamond structure. These calculations were carried out first by Williamson et al (111) with VQMC calculations, using pseudopotentials and a plane wave basis set for the four valence electrons of each atom. Simulation cell sizes were varied in $n \times n \times n$ multiples of the primitive unit cell with $n = 2, 3, 4,$ and 5 corresponding to 16, 54, 128, and 250 atoms or 64, 208, 512, and 1000 electrons, respectively. With these calculations, Williamson et al tested a new model periodic Coulomb interaction and found it to be far superior to the

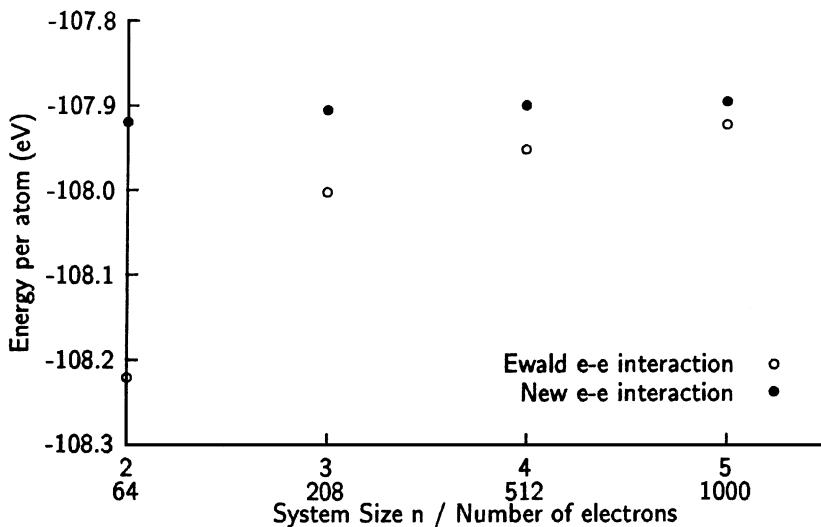


Figure 8 Variation of energy (per atom) with simulation cell size n in calculations by Williamson et al (111) for silicon crystal. The values $n = 2, 3, 4,$ and 5 correspond to 64, 208, 512, and 1000 valence electrons in the cell.

Ewald model in eliminating Coulomb finite-size effects for VQMC calculations (as well as for HF calculations).

DQMC calculations for the same silicon structure and simulation with $n = 1, 2, 3, 4, 5,$ and corresponding to 2, 16, 54, 128, and 250 atoms or 8, 64, 208, 512, and 1000 electrons, respectively, were reported by Kent et al (112) in early 1999. The calculations were fixed-node calculations with pseudopotentials representing the inner-shell electrons. In this case, Kent et al (112) extended the model periodic Coulomb interaction to all Coulomb interactions in the system. With DQMC, the model interaction required the charge density in advance of a calculation, but this was approximated without difficulty. Results for the ground state are shown in Figure 8.

The total energies in the DQMC calculations of Kent et al were determined with a statistical accuracy of ± 0.02 eV per atom. That is <1 millihartree per atom.

The cohesive energy obtained for silicon was 4.63 (2) eV per atom—a value very close to the experimental value of 4.62 (8) eV per atom—indicating that the DQMC method can give cohesive energies within 0.1 eV for such systems (3). That is an accuracy of 5 millihartree per atom for 1000 atoms.

We note that one effect of the calculations with 1000 electrons was to show that the extended model periodic potential of Kent et al (112) gives accurate results with fewer electrons.

(110) SURFACE OF GALLIUM ARSENIDE (192 VALENCE ELECTRONS)

The gallium arsenide surface has been investigated in VQMC calculations by Bahnsen et al (113), as reported in 1999. These calculations represent the first attempts at treating GaAs, which serves as a prototype for semiconductor surfaces of all types. The system considered was a cell of six layers, each containing four Ga and four As atoms for a total of 48 atoms and 192 valence electrons. The inner-shell electrons were included with nonlocal pseudopotentials.

Similar systems have been treated previously with DFT, using the LDA or one of the generalized-gradient approximations. The complex inhomogeneous nature of surfaces and the absence of detailed experimental information on these surfaces make it very difficult to judge the success of DFT for these systems. QMC offers an alternative.

The calculations were carried out for the geometry of the relaxed (110) surface of GaAs, in the geometry proposed by Duke et al (114). The boundaries were those of a “finite-layer geometry” with periodic conditions parallel to the surface and a finite number (six) of layers that are perpendicular to the surface. A two-dimensional Ewald summation technique was used, and finite-size effects were not investigated.

The trial wave function for the VQMC was of the Slater-Jastrow type, with the Slater determinant consisting of doubly occupied orbitals similar to those of earlier bulk calculations (115) but with alterations to incorporate dangling bond orbitals. The several parameters of the wave function were optimized sequentially to minimize the expectation value of the energy. Although the authors were able to make a qualitative interpretation of the physics involved, for example, in terms of the direction of the dangling bonds, a more detailed analysis would require more lengthy calculations of higher accuracy. Nevertheless, they have provided a successful first attempt at treating surfaces such as these by QMC methods.

CONCLUDING REMARKS

The success of QMC methods for systems both large and small has led Foulkes et al (3) to point out that “...the accuracy of the VMC and DMC methods is *systematic*: the same accuracy pattern has been demonstrated for atoms, molecules, solids, and surfaces.” Perhaps one might anticipate that, as any general method approaches exact solutions to the Schrödinger equation, the accuracy pattern becomes systematic. We are indeed fortunate to be able to consider such questions.

ACKNOWLEDGMENTS

Support by the US National Science Foundation (grants CHE-9411181 and DGE-9354958) and Deutsche Forschungsgemeinschaft (AL) is gratefully acknowledged.

Visit the Annual Reviews home page at www.AnnualReviews.org

LITERATURE CITED

1. Lester WA Jr, Hammond BL. 1990. *Annu. Rev. Phys. Chem.* 41:283–311
2. Bergström R. 1996. *Int. J. Quantum Chem.* 60:791
3. Foulkes WMC, Mitas L, Needs R, Rajagopal G. 2000. *Rev. Mod. Phys.* In press
4. Hammond BL, Lester WA Jr, Reynolds PJ. 1994. *Monte Carlo Methods in Ab Initio Quantum Chemistry* Singapore: World Scientific 304 pp.
5. Anderson JB. 1999. *Rev. Comput. Chem.* 13:133–81
6. Ceperley DM, Mitas L. 1996. *Adv. Chem. Phys.* 93:1–38
7. Anderson JB. 1995. In *Quantum Mechanical Electronic Structure Calculations with Chemical Accuracy*, ed. SR Langhoff, pp. 1–45. Dordrecht: Kluwer
8. Anderson JB. 1995. *Int. Rev. Phys. Chem.* 14:85–112
9. Mitas L. 1995. In *Electronic Properties of Solids Using Cluster Methods*, ed. TA Kaplan, SD Mahanti, pp. 131–41. New York: Plenum
10. Suhm MA, Watts RO. 1991. *Phys. Rep.* 204:293–329
11. Ceperley DM. 1986. *J. Stat. Phys.* 43:815–26
12. Shlyakhter Y, Sokolova S, Lüchow A, Anderson JB. 1999. *J. Chem. Phys.* 110:10725–29
13. Head-Gordon M. 1996. *J. Phys. Chem.* 100:13213–25
14. Anderson JB. 1975. *J. Chem. Phys.* 63:1499–503
15. Metropolis N, Ulam S. 1949. *J. Am. Stat. Assoc.* 44:335–41
16. Grimm RC, Storer RG. 1971. *J. Comput. Phys.* 7:134–56
17. Reynolds PJ, Ceperley DM, Alder BJ, Lester WA Jr. 1982. *J. Chem. Phys.* 77:5593–603
18. Umrigar CJ, Nightingale MP, Runge KJ. 1993. *J. Chem. Phys.* 99:2865–90
19. Anderson JB. 1976. *J. Chem. Phys.* 65:4121–27
20. Ceperley DM, Alder BJ. 1984. *J. Chem. Phys.* 81:5833–44
21. Conroy H. 1964. *J. Chem. Phys.* 41:1331–35
22. Hurley MM, Christiansen PA. 1987. *J. Chem. Phys.* 86:1069–70
23. Hammond BL, Reynolds PJ, Lester WA Jr. 1987. *J. Chem. Phys.* 87:1130–36
24. Buch V. 1992. *J. Chem. Phys.* 97:726–29
25. Metropolis N, Rosenbluth AW, Rosenbluth MN, Teller AM, Teller E. 1953. *J. Chem. Phys.* 21:1087–92
26. McMillan WL. 1965. *Phys. Rev.* 138:442–51
27. Kalos MH, Whitlock PA. 1986. In *Monte Carlo Methods*, pp. 73–86. New York: Wiley
28. Morse PM, Feshbach H. 1953. In *Methods of Theoretical Physics*, Vol. 1, Ch. 7. New York: McGraw-Hill
29. Kalos MH. 1962. *Phys. Rev.* 128:1791–95
30. Brezinsky K. 1986. *Prog. Energy Combust. Sci.* 3:1–24
31. Emdee JL, Brezinsky K, Glassman I. 1992. *J. Phys. Chem.* 96:2151–61
32. Grossman JC, Lester WA Jr, Louie SG. 1999. *J. Am. Chem. Soc.* In press
33. Grossman JC, Lester WA Jr, Louie SG. 1999. *Mol. Phys.* 96:629–32
34. Weinhold PG, Hrovat DA, Borden WT, Lineberger WC. 1996. *Science* 272:1456–59
35. Grossman JC, Mitas L. 1997. *Phys. Rev. Lett.* 79:4353–56
36. Weltner W Jr, Van Zee RJ. 1989. *Chem. Rev.* 89:1713–47

37. Martin JML, François J-P, Gijbels R. 1993. *J. Mol. Struct.* 294:21–24
38. Van Orden A, Saykally RJ. 1998. *Chem. Rev.* 98:2313–57
39. Jones RO, Seifert G. 1997. *Phys. Rev. Lett.* 79:443–46
40. Parasuk V, Almlöf J. 1991. *Chem. Phys. Lett.* 184:187–90
41. Murphy RB, Friesner RA. 1998. *Chem. Phys. Lett.* 288:403–7
42. Grossman JC, Mitas L, Raghavachari K. 1995. *Phys. Rev. Lett.* 75:3870–73
43. Martin JML, El-Yazal J, François J-P. 1996. *Chem. Phys. Lett.* 248:345–52
44. Taylor PR, Bylaska E, Weare JH, Kawai R. 1995. *Chem. Phys. Lett.* 235:558–63
- 44a. Bylaska B, Taylor PR, Kawai R, Weare JH. 1996. *J. Phys. Chem.* 100:6966–72
45. Raghavachari K, Stout DL, Odom GK, Scuseria GE, Pople JA, et al. 1993. *Chem. Phys. Lett.* 214:357–61
46. Slanina Z, Adamowicz L. 1992. *Thermochim. Acta* 205:299–306
- 46a. Slanina Z, Adamowicz L. 1993. *Fullerene Sci. Tech.* 1:1–9
47. Wang Z, Day P, Pachter R. 1996. *Chem. Phys. Lett.* 248:121–26
48. Sokolova S, Lüchow A, Anderson JB. 2000. *Chem. Phys. Lett.* In press
49. Kent PRC, Towler MD, Needs RJ, Rajagopal G. 2000. *Phys. Rev. Lett.* In press
50. Hartmann M, Miller RE, Toennies JP, Vilesov AF. 1995. *Phys. Rev. Lett.* 75:1566–69
51. Grebenev S, Toennies JP, Vilesov AF. 1998. *Science* 279:2083–86
52. Toennies JP, Vilesov AF. 1998. *Annu. Rev. Phys. Chem.* 49:1–41
53. Nauta K, Miller RE. 1999. *Science* 238:3426–33
54. Nauta K, Miller RE. 1999. *J. Chem. Phys.* 111:1895–97
55. Barnett RN, Whaley KB. 1993. *J. Chem. Phys.* 99:9730–44
56. Barnett RN, Whaley KB. 1995. *J. Chem. Phys.* 102:2290
- 56a. Chin SA, Krotscheck E. 1995. In *Recent Progress in Many-Body Theories* ed. E Schachinger, H Mitter, H Sormann, Vol. 4, pp. 85–92. New York: Plenum 4:85–92
- 56b. McMahon MA, Barnett RN, Whaley KB. 1996. *J. Chem. Phys.* 104:5080–93
57. Kwon Y, Ceperley DM, Whaley KB. 1996. *J. Chem. Phys.* 104:2341–48
58. Lee E, Farrelly D, Whaley KB. 1999. *Phys. Rev. Lett.* 83:3812–15
59. Barnett RN, Whaley KB. 1992. *J. Chem. Phys.* 96:2953–65
60. Bacic Z, Kennedy-Manduziuk M, Moskowitz JW, Schmidt KE. 1992. *J. Chem. Phys.* 97:6472–80
61. McMahon MA, Whaley KB. 1995. *J. Chem. Phys.* 103:2561–71
62. Blume D, Lewerenz M, Huisken F, Kaloudis M. 1996. *J. Chem. Phys.* 105:8666–83
63. Bressanini D, Mella M, Morosi G. 1998. *Phys. Rev. A* 57:1678–85
64. Bressanini D, Mella M, Morosi G. 1998. *J. Chem. Phys.* 108:4756–60
- 64a. 1998. Bressanini D, Mella M, Morosi G. 1998. *J. Chem. Phys.* 109:1716–20
65. Bressanini D, Mella M, Morosi G. 1998. *J. Chem. Phys.* 109:5931–34
66. Kao CM, Cade PE. 1984. *J. Chem. Phys.* 80:3234–45
67. Tachikawa M, Sainowo H, Iguchi K, Suzuki K. 1994. *J. Chem. Phys.* 101:5925–28
- 67a. Schrader DM. 1996. *J. Chem. Phys.* 104:3147
68. Saito T, Tachikawa M, Ohe C, Iguchi K, Suzuki K. 1996. *J. Phys. Chem.* 100:6057–60
69. Yoshida T, Miyako G, Jiang N, Schrader DM. 1996. *Phys. Rev. A* 54:964–66
70. Curtiss LA, Raghavachari K, Trucks GW, Pople JA. 1991. *J. Chem. Phys.* 94:7221–30

71. Lüchow A, Anderson JB. 1996. *J. Chem. Phys.* 105:7573–78
72. Schmidt KE, Moskowitz JW. 1990. *J. Chem. Phys.* 93:4172–78
73. Guo BC, Kerns KP, Castleman AW Jr. 1992. *Science* 255:1411–13
74. Guo BC, Wei W, Purnell J, Buzza S, Castleman AW Jr. 1992. *Science* 256:515–16
75. Guo BC, Wei W, Purnell J, Buzza S, Castleman AW Jr. 1992. *Science* 256:818–20
76. Chen H, Feyereisen M, Long XP, Fitzgerald G. 1993. *Phys. Rev. Lett.* 71:1732–35
77. Methfessel M, van Schilfgaarde M, Scheffler M. 1993. *Phys. Rev. Lett.* 70:29–32
78. Reddy BV, Khanna SN, Jena P. 1992. *Science* 258:1640–43
79. Hack MD, Maclagan RGA, Scuseria GE. 1996. *J. Chem. Phys.* 104:6628–30
80. Sokolova S, Lüchow A. 2000. *Chem. Phys. Lett.* 320:421–24
81. Moore CE. 1949. *Atomic Energy Levels. U.S. Bureau of Standards Circ. 467*, Vol. 1, pp. 273–90. Washington, DC: U.S. Bureau Stand.
82. Pugliano N, Saykally RJ. 1992. *Science* 257:1937–40
83. Liu K, Brown MG, Carter C, Saykally RJ, Gregory JK, Clary DC. 1996. *Nature* 381:501–3
84. Huisken F, Kaloudis M, Kulcke A. 1996. *J. Chem. Phys.* 104:17–25
85. Buck U, Ettischer I, Melzer M, Buch V, Sadlej J. 1998. *Phys. Rev. Lett.* 80:2578–81
86. Brudermann J, Melzer M, Buck U, Kazimirski JK, Sadlej J, Buch V. 1999. *J. Chem. Phys.* 110:10649–52
87. Buch V. 1992. *J. Chem. Phys.* 96:3814–23
88. Gregory JK, Clary DC. 1995. *J. Chem. Phys.* 103:8924–30
89. Sadlej J, Buch V, Kazimirski JK, Buck U. 1999. *J. Phys. Chem. A* 103:4933–47
90. Liu K, Loeser JG, Elrod MJ, Host BC, Rzepiela JA, et al. 1994. *J. Am. Chem. Soc.* 116:3507–12
91. Sun H, Watts RO. 1990. *J. Chem. Phys.* 92:603–16
92. Quack M, Suhm MA. 1991. *J. Chem. Phys.* 95:28–59
93. Severson M, Buch V. 1999. *J. Chem. Phys.* 111:10866–75
94. Gregory JK, Clary DC, Liu K, Brown MG, Saykally RJ. 1997. *Science* 275:814–17
95. Gregory JK. 1998. *Chem. Phys. Lett.* 282:147–51
96. Fahy S, Wang XW, Louie SG. 1988. *Phys. Rev. Lett.* 61:1631–34
97. Fahy S, Wang XW, Louie SG. 1990. *Phys. Rev. B* 42:3503–22
98. Mitas L, Martin RM. 1994. *Phys. Rev. Lett.* 72:2438–41
99. Mitas L. 1996. *Comput. Phys. Commun.* 96:107–17
100. Williamson AJ, Hood RQ, Needs RJ, Rajagopal G. 1998. *Phys. Rev. B* 57:12140–44
101. Rajagopal G, Needs RJ, Kenny S, Foulkes WMC, James A. 1994. *Phys. Rev. Lett.* 73:1959–62
102. Borrmann W, Fulde P. 1987. *Phys. Rev. B* 35:9569–79
103. Rohlfing M, Krüger P, Pollmann J. 1993. *Phys. Rev. B* 48:17791–805
104. Hellwege K-H, Madelung O, eds. 1982. *Numerical Data and Functional Relationships in Science and Technology*. Berlin: Springer
105. Kent PRC, Hood RQ, Towler MD, Needs RJ, Rajagopal G. 1998. *Phys. Rev. B* 57:15293–302
106. Day OW, Smith DW, Garrod C. 1974. *Int. J. Quantum Chem. Symp.* 8:501–9
107. Morrell MM, Parr RG, Levy M. 1975. *J. Chem. Phys.* 62:549–54
108. Malatesta A, Fahy S, Bachelet GB. 1997. *Phys. Rev. B* 56:12201–10
109. Hamann DR, Schlüter M, Chiang C. 1979. *Phys. Rev. Lett.* 43, 1494–97
110. Knittle E, Wentzcovitch R, Jeanloz R, Cohen ML. 1989. *Nature* 337:349–52
111. Williamson AJ, Rajagopal G, Needs RJ, Fraser LM, Foulkes WMC, et al. 1997. *Phys. Rev. B* 55:R4581–R4584

112. Kent PRC, Hood RQ, Williamson AJ, Needs RJ, Foulkes WMC, Rajagopal G. 1999. *Phys. Rev. B* 59:1917–29
113. Bahnsen R, Schulz D, Schattke W, Redmer R. 1999. *Czech. J. Phys.* 49:1519–24
114. Duke CB, Richardson SL, Paton P, Kahn A. 1983. *Surf. Sci.* 127:L135–L143
115. Eckstein H, Schattke W, Reigrotzki M, Redmer R. 1996. *Phys. Rev. B* 54:5512–15



CONTENTS

Fifty Years in Physical Chemistry: Homage to Mentors, Methods, and Molecules, <i>Dudley Herschbach</i>	1
SURFACE PLASMON RESONANCE IMAGING MEASUREMENTS OF ULTRATHIN ORGANIC FILMS, <i>Jennifer M. Brockman, Bryce P. Nelson, Robert M. Corn</i>	41
Delayed Ionization and Fragmentation En Route to Thermionic Emission: Statistics and Dynamics, <i>E. E. B. Campbell, R. D. Levine</i>	65
Spatially Heterogeneous Dynamics in Supercooled Liquids, <i>M. D. Ediger</i>	99
Generalized Born Models of Macromolecular Solvation Effects, <i>Donald Bashford, David A. Case</i>	129
Chemical Dynamics at Metal Surfaces, <i>John C. Tully</i>	153
Peptides and Proteins in the Vapor Phase, <i>Martin F. Jarrold</i>	179
Effective Interactions Between Electric Double Layers, <i>Jean-Pierre Hansen, Hartmut Löwen</i>	209
Transient Laser Frequency Modulation Spectroscopy, <i>Jean-Pierre Hansen, Hartmut Löwen</i>	243
Motion and Disorder in Crystal Structure Analysis: Measuring and Distinguishing Them, <i>H. B. Bürgi</i>	275
Quantitative Atom-Atom Potentials from Rotational Tunneling: Their Extraction and Their Use, <i>M. R. Johnson, G. J. Kearley</i>	297
Decoding the Dynamical Information Embedded in Highly Mixed Quantum States, <i>John C. Keske, Brooks H. Pate</i>	323
Large-Scale Shape Changes in Proteins and Macromolecular Complexes, <i>Michael E. Wall, Stephen C. Gallagher, Jill Trehwella</i>	355
Reflection Absorption Infrared Spectroscopy and the Structure of Molecular Adsorbates on Metal Surfaces, <i>Michael Trenary</i>	381
The Dynamics of Noble Gas-Halogen Molecules and Clusters, <i>Andreas Rohrbacher, Nadine Halberstadt, Kenneth C. Janda</i>	405
Molecular Dynamics Simulation of Nucleic Acids, <i>Thomas E. Cheatham III, Peter A. Kollman</i>	435
Chemistry and Microphysics of Polar Stratospheric Clouds and Cirrus Clouds, <i>Mark A. Zondlo, Paula K. Hudson, Anthony J. Prenni, Margaret A. Tolbert</i>	473
Monte Carlo Methods in Electronic Structures for Large Systems, <i>Arne Lüchow, James B. Anderson</i>	501
Thermodynamics of the Size and Shape of Nanocrystals: Epitaxial Ge on Si(001), <i>R. Stanley Williams, Gilberto Medeiros-Ribeiro, Theodore I. Kamins, Douglas A. A. Ohlberg</i>	527
Semiclassical Calculation of Chemical Reaction Dynamics via Wavepacket Correlation Functions, <i>David J. Tannor, Sophya Garashchuk</i>	553
Self-Assembled Ceramics Produced by Complex-Fluid Templatation, <i>Daniel M. Dabbs, Ilhan A. Aksay</i>	601
Theoretical Studies of Atomic-Scale Processes Relevant to Crystal Growth, <i>Hannes Jónsson</i>	623
New Technologies in Electron Spin Resonance, <i>Jack H. Freed</i>	655
Multidimensional Femtosecond Correlation Spectroscopies of Electronic and Vibrational Excitations, <i>Shaul Mukamel</i>	691

Structures and Dynamics of Molecules on Liquid Beam Surfaces, <i>Tamotsu Kondow, Fumitaka Mafuné</i>	731
Effects of High Pressure on Molecules, <i>Russell J. Hemley</i>	763